LETTER TO THE EDITOR OPEN

Cryo-EM structure of constitutively active human Frizzled 7 in complex with heterotrimeric G_s

Cell Research (2021) 31:1311–1314; https://doi.org/10.1038/s41422-021-00525-6

Dear Editor,

The ten mammalian Frizzleds (FZD_{1-10}) belong to the class F of G protein-coupled receptors (GPCRs) and mediate WNT signaling through interaction with transducer proteins including Dishevelled (DVL) or heterotrimeric G proteins.[1] Their involvement in human disease has put FZDs at the forefront of drug targets, especially anti-cancer therapy.[2] However, no drugs have been developed for efficient pharmacological modulation of FZDs, partially owing to the limited understanding of FZD structure and activation mechanisms.[1,3] Among class F, FZD_7 is intensively pursued due to its relevance in various tumor models, particularly in intestinal cancers.[4] Detailed structures of the receptor complexes would allow for structure-guided discovery of new drug candidates. FZD_{1-10} share structural similarity with the related class F member Smoothened (SMO), which mediates Hedgehog signaling and is a validated target for cancer therapy.[2] In an effort to understand the structural basis of FZD activation and transducer interaction, we solved the structure of human FZD_7 in complex with heterotrimeric mini G_s (mG_s).[5]

Based on the evidence that FZD_7 interacts with G_s to mediate muscle hypertrophy,[6,7] we assessed its ability to activate heterotrimeric G_s independently of WNT stimulation. Co-expression of FZD_7 with a bioluminescence resonance energy transfer (BRET)-based G_s biosensor,[8] reporting the rearrangement or dissociation of $G\alpha_s$ and $G\beta\gamma$ following receptor engagement and G protein activation, revealed that FZD_7 exhibits constitutive activity similar to the class A β_2-adrenoceptor (Fig. 1a; Supplementary information, Fig. S1a, b). Using an analogous assay that measures activity-dependent $G\alpha_s$ translocation (Supplementary information, Fig. S1c), we found that the constitutive activity of FZD_7 correlates with increased receptor expression (Supplementary information, Fig. S1d, e). Given the robust constitutive activity of FZD_7 towards G_s, we reconstituted purified, full-length human FZD_7, heterotrimeric mG_s and Nanobody35 (Nb35), which stabilizes the nucleotide-free $G\alpha_s$ and $G\beta$ subunits,[9] in the absence of ligand and obtained pure complexes following size exclusion chromatography (Supplementary information, Fig. S2). The final complex was composed of FZD_7, $mG\alpha_s$, $G\beta$, $G\gamma$ and Nb35, which could be clearly identified by 2D classification (Fig. 1b; Supplementary information, Fig. S2d). We used single-particle cryo-EM analysis to determine the 3D structure of this complex. After several rounds of classification and auto-refinement, the resolution of the final structure reached 3.2 Å allowing us to build an atomic model based on the density map (Fig. 1c; Supplementary information, Figs. S3–S5, Table S1).

In accordance with the functional evidence for constitutive activity, the FZD_7–mG_s complex structure provides the structural basis for ligand-independent G protein coupling (Fig. 1c). The interface between FZD_7 and mG_s is dominated by the distal C-terminal segment of the α5-helix in $mG\alpha_s$ (Fig. 1d, e). The C-terminal leucine residues ($L393^{H5.25}$, $L394^{H5.26}$; superscripts refer to the residue position in the common Gα numbering scheme for G proteins/GPCRdb) are inserted into the helical bundle of the receptor. $L393^{H5.25}$ and $L394^{H5.26}$ establish extensive interactions with FZD_7 residues yielding a locally converged network that stabilizes the complex (Fig. 1e). The terminal carboxyl group of $L394^{H5.26}$ in $mG\alpha_s$ forms an ionic bond with $K466^{6.28}$, and residues $R281^{ICL1}$, $K552^{8.49}$ and $R470^{6.32}$ of FZD_7 are located in close proximity (superscript numbers refer to the Ballesteros and Weinstein numbering system). $Y391^{H5.23}$ forms a hydrogen bond with the backbone of $W369^{ICL2}$. Residues $I450^{5.72}$, $I453^{5.75}$ and $M454^{5.76}$ of FZD_7 form a hydrophobic cleft accommodating $L388^{H5.20}$. Furthermore, $R385^{H5.17}$ forms an ionic bond with D457 in ICL3, further strengthening the interaction between the α5-helix and FZD_7. In summary, the recognition of $G\alpha_s$ by FZD_7 is primarily governed by a network of hydrogen bonding and electrostatic interactions contributed from the C-terminal segment of the α5-helix ($D381^{H5.13}$-$L394^{H5.26}$), among which, interactions with $L394^{H5.26}$ lock the α5-helix tail in an uncoiled, elongated conformation (Fig. 1e).

The placement of the α5-helix of $mG\alpha_s$ in the core of FZD_7 stabilizes an open FZD_7 conformation. We compared the FZD_7–mG_s structure with the available inactive-state FZD_4 crystal structure (PDB: 6BD4) and the inactive-state FZD_5 cryo-EM structure (PDB: 6WW2) and observed a clear outward bending of TM6 and an inward shift of TM5 at the cytoplasmic side (Fig. 1f–h)—a conformational change characteristic of active-state class A and B GPCRs. This helical rearrangement is achieved through interaction of TM6 and TM5 with mG_s and opening of the molecular switch between TM6 and TM7 ($R^{6.32}$/$W^{7.55}$; Fig. 1i).[7] Comparing inactive FZD_4 with FZD_7–mG_s reveals that the extracellular portion of TM6 of FZD_7 extends above the surface of the lipid bilayer at an angle of 45° (Supplementary information, Figs. S6, S7), similar to what we have predicted in previous models[10] and in contrast to the almost 90° bending in the FZD_4 structure.[11] Moreover, conserved cysteines within the hinge domain form disulfide bonds to both stabilize its structure and to link it with ECL1 (C210–C230; C234–$C315^{ECL1}$) (Supplementary information, Fig. S6).[12]

To better understand the activation mechanism of FZD_7 and G protein coupling to class F receptors, we compared the FZD_7–mG_s structure with the agonist (24(*S*), 25-epoxycholesterol)-bound structure of SMO–G_i[13] (PDB: 6OT0). The helical arrangement at the upper portion of the FZD_7 transmembrane core is more compact, presumably due to the absence of ligand (Supplementary information, Fig. S7). At the lower portion of TM6, substantially distinct conformations are observed between the SMO–G_i and FZD_7–mG_s structures. Most strikingly, TM6 in SMO–G_i undergoes a parallel outward movement compared to inactive SMO, whereas TM6 in the FZD_7–mG_s complex accomplishes a

Received: 10 March 2021 Accepted: 28 May 2021
Published online: 8 July 2021

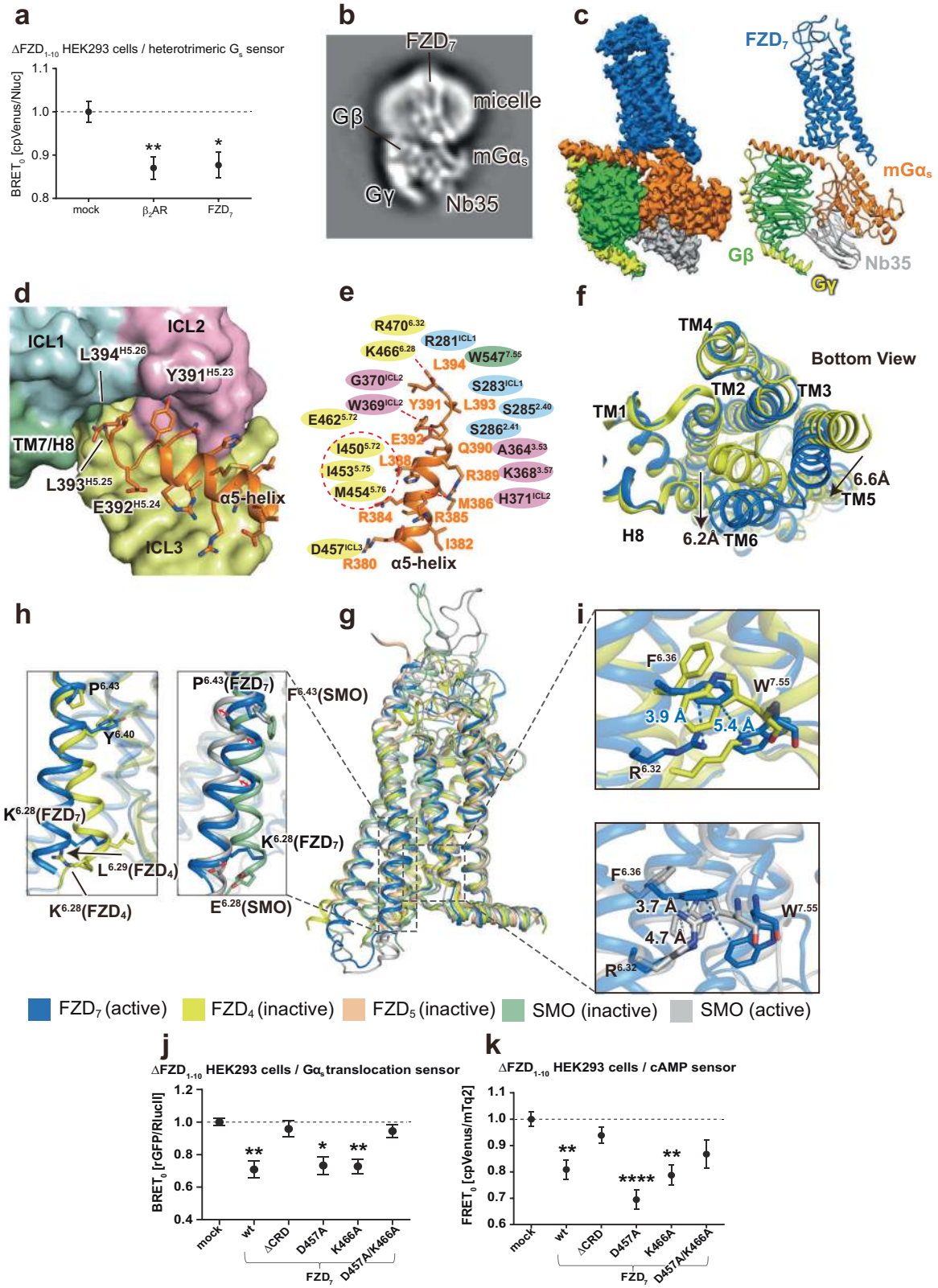

similar displacement of the cytoplasmic portion through a kink in the helix (Fig. 1h). The ionic interactions between TM6, ICL3 and the α5-helix of $mG\alpha_s$ ($K466^{6.28}$–$L394^{H5.26}$ and $D457$–$R385^{H5.17}$) are likely to be the main contributors in maintaining this kink. In addition, $Y478^{6.40}$ forms π–π interaction with $W354^{3.43}$ to further maintain the bent TM6 conformation (Supplementary information, Fig. S7).

While the most evident structural rearrangements relate to TM6, additional positional shifts of TM2, TM3, TM4 and TM5 in the FZD_7–mG_s complex are observed when compared to the SMO–G_i

Fig. 1 Structure of constitutively active FZD_7 in complex with heterotrimeric mG_s. a Normalized $BRET_0$ values of ΔFZD_{1-10} HEK293 cells transiently co-transfected with the G_s BRET sensor along with either negative control (mock), the β_2-adrenoceptor (β_2AR) or FZD_7. Data are represented as the means ± SEM of raw $BRET_0$ that were obtained from simple linear regression of five independent experiments measured in quadruplicates shown in Supplementary information, Fig. S1A and normalized to the negative control. $^*P < 0.05$; $^{**}P < 0.01$ (one-way ANOVA followed by Sidak's multiple comparison). **b** An annotated 2D class average of FZD_7–mG_s–Nb35 complex. **c** Overall density map and atomic model of FZD_7–mG_s–Nb35 complex (CRD was omitted due to linker flexibility). FZD_7, blue; $mG\alpha_s$, orange; Gβ, green; Gγ, yellow; Nb35, gray. **d** Insertion of the α5-helix ($mG\alpha_s$, orange) into FZD_7 helical bundle represented as surface (ICL1, blue; ICL2, pink; ICL3, yellow; TM7/H8, green). **e** Schematics of interactions between FZD_7 and α5-helix. Hydrogen bonds are shown as red dashed lines. The red circle represents the hydrophobic interaction network. Yellow shades indicate residues that reside in TM5/6/ICL3; pink, TM3/4/ICL2; blue, TM1/2/ICL1; green, TM7/H8. **f** Superposition of FZD_7 (blue) and FZD_4 (yellow) structures, viewed from the intracellular side (bottom view). **g** Superposition of the active FZD_7 structure (blue) with the inactive FZD_4 (PDB: 6BD4, yellow), inactive FZD_5 (PDB: 6WW2, light pink), active SMO (PDB: 6OT0, gray) and inactive SMO (PDB: 5V57, green) structures. **h** Comparison of the cytoplasmic portion of TM6 (from $K^{6.28}$ to $P^{6.43}$) in FZD_7, FZD_4, active SMO and inactive SMO structures. **i** $R^{6.32}$, $F^{6.36}$, $W^{7.55}$ network in FZD_7, FZD_4 and active SMO structures. Blue dashed lines indicate the distance of $F^{6.36}$–$W^{7.55}$ and $F^{6.36}$–$R^{6.32}$ in FZD_7. Gray dashed lines indicate the distance of $R^{6.32}$–$W^{7.55}$ and $W^{7.55}$–$F^{6.36}$ in active SMO structure. **j** Normalized $BRET_0$ values of ΔFZD_{1-10} HEK293 cells transiently co-transfected with rGFP-CAAX and $G\alpha_s$-67-*R*lucII, along with either negative control (mock), wild-type FZD_7, ΔCRD-FZD_7 or the indicated FZD_7 mutants. Data are represented as the means ± SEM of raw $BRET_0$ that were obtained from simple linear regression of four independent experiments measured in quadruplicates shown in Supplementary information, Fig. S11b and normalized to the negative control. $^{**}P < 0.01$; $^{***}P < 0.001$ (one-way ANOVA followed by Tukey's multiple comparison). **k** Normalized $FRET_0$ values of ΔFZD_{1-10} HEK293 cells transiently co-transfected with the FRET-based cAMP biosensor along with either negative control (mock), wild-type FZD_7, ΔCRD-FZD_7 or the indicated FZD_7 mutants. Data are represented as the means ± SEM of raw $FRET_0$ that were obtained from simple linear regression of five independent experiments measured in quadruplicates shown in Supplementary information, Fig. S11c and normalized to the negative control. $^{**}P < 0.01$; $^{****}P < 0.0001$ (one-way ANOVA followed by Sidak's multiple comparison).

complex. These four helices constitute a more compact bundle in the FZD_7–mG_s structure, partially stabilized by a network of π interactions (Supplementary information, Fig. S7e). In a cooperative manner, these interactions promote the cytoplasmic portion of TM4 shifting inward by ~2 Å (comparing the Cα of $L383^{4.47}$ in FZD_7–mG_s with corresponding $L362^{4.47}$ in SMO–G_i complex structures) (Supplementary information, Fig. S7f, black arrow).

A conserved molecular switch between TM6 and TM7 was previously identified for all class F GPCRs, maintaining the receptor in an inactive conformation (observed as a hydrogen-bonding distance between $R^{6.32}$ and the backbone of $W^{7.55}$) in all inactive class F receptor structures.[7] The polar interactions between $R^{6.32}$ and $W^{7.55}$ are broken in active SMO–G_i and the FZD_7–mG_s complexes, resulting in a 6.4 Å distance between $R470^{6.32}$ and $W547^{7.55}$ in the FZD_7–mG_s complex (Fig. 1f, h).[7]

To explore the conformational dynamics around the open and active FZD_7 structure, we performed molecular dynamics (MD) simulations of FZD_7 in complex with mG_s393[5] (Supplementary information, Fig. S8). Monomeric mG_s facilitated MD simulations due to its small size while minimizing the effect on receptor dynamics. These MD simulations allowed us to monitor general receptor integrity and the status of the molecular switch by assessing the angle of the kinked TM6 and the distance between $R470^{6.32}$ and $W547^{7.55}$. The overall hallmark of FZD_7 activation — the kink in TM6 — is maintained over the time course of the simulation (measured as an angle between the backbone nitrogen atoms of $V485^{6.47}$, $P481^{6.43}$ and $E462^{6.24}$). $P^{6.43}$ is fully conserved among the FZD paralogues, but not in SMO ($F^{6.43}$) (Supplementary information, Fig. S9). Analogous to $P^{6.50}$ and $P^{6.47}$ in class A and B receptors, respectively (Supplementary information, Fig. S10), $P481^{6.43}$ is likely to contribute to the observed outward movement of the lower part of TM6[14] (Fig. 1f, h). In the MD trajectories, the conformational changes of TM6 are manifested by the disruption of the molecular switch and a rearrangement of an extended aromatic network stabilizing the active receptor conformation (Supplementary information, Fig. S8). $R470^{6.32}$ and the backbone oxygen atom of $W547^{7.55}$ remain at over 8 Å distance throughout the simulation, rendering hydrogen bonding impossible between these two residues. Instead, $R470^{6.32}$ is frequently bound with the carboxyl terminus of $L^{H5.26}$ of $mG\alpha_s$. Interestingly, $R470^{6.32}$ remains within hydrogen-bonding distance to the carboxyl terminus of $L^{H5.26}$ more often than $K466^{6.28}$, indicating that these positively charged residues lock the carboxyl tail between them (Supplementary information, Fig. S8d). This could contribute to the observed non-helical conformation of the tail of the α5-helix.

To gather functional evidence for the FZD_7–mG_s interface and its role in maintaining the constitutive activity of FZD_7 towards G_s, we employed a mutagenesis-based approach in combination with assessment of $G\alpha_s$ translocation and cAMP production as functional readouts of G_s-dependent signaling. We focused on D457 (in ICL3) and $K466^{6.28}$, which interact with the α5-helix of $mG\alpha_s$. Mutating either D457 or $K466^{6.28}$ to alanine alone did not affect the constitutive activity of FZD_7 on G_s translocation or cAMP production (Fig. 1j, k; Supplementary information, Figs. S11, S12). However, the double mutant D457A/$K466^{6.28}$A abrogated FZD_7 constitutive activity towards G_s, suggesting that these mutations collectively interfere with G protein coupling. In contrast, the double mutant did not affect the ability of FZD_7 to mediate WNT-induced activation of the WNT/β-catenin pathway as assessed by the TOPFlash reporter assay (Supplementary information, Fig. S13), underlining the concept of conformational selection for DVL-dependent signaling over G protein coupling as has been suggested previously.[7,15]

Although the CRD could not be resolved in the present structure, we observed that removal of the CRD (ΔCRD-FZD_7) resulted in the inability to reconstitute the receptor–mG_s complex in vitro to the same extent as that of full-length FZD_7 (Supplementary information, Fig. S14). Thus, we surmised that the CRD is required for FZD_7–mG_s complex stability and that removal of the CRD could decrease constitutive activity. Therefore, we assessed the ability of the ΔCRD-FZD_7 construct to functionally couple to G_s by assessing $G\alpha_s$ translocation and cAMP production (Fig. 1j, k). Removal of the CRD blunted the constitutive activity towards G_s signaling as evidenced by the lack of $G\alpha_s$ translocation and cAMP production. These data underline the requirement for the CRD to maintain constitutive activity of FZD_7 towards heterotrimeric G proteins through intramolecular allostery.

In conclusion, we report the cryo-EM structure of FZD_7–mG_s demonstrating how constitutive activity feeds into downstream signaling via heterotrimeric G proteins. With respect to the overall diversity among GPCRs, FZD_7 has evolved a unique way to maintain certain homologous movements consistent with class A and B GPCR activation, while adapting its class-specific architecture to mediate G protein activation. While the classical hallmarks of G protein engagement are present in our structure, several differences can be found at the interface between the receptor and the G protein suggesting that FZDs harbor their own

selectivity determinants for heterotrimeric G proteins. In short, the present structure of constitutively active FZD_7–mG_s, alongside previously published inactive structures of FZD_4 and FZD_5, opens the door to more accurate modeling of other FZDs and a platform for in silico drug discovery, which will aid in the discovery of new treatments to help those afflicted with diseases of WNT-FZD signaling.

Lu Xu[1,2,3,4,9], Bo Chen[1,9], Hannes Schihada[5,9], Shane C. Wright[5,6,9], Ainoleena Turku[5,8], Yiran Wu[1], Gye-Won Han[7], Maria Kowalski-Jahn[5], Pawel Kozielewicz[5], Carl-Fredrik Bowin[5], Xianjun Zhang[1,2,3,4,7], Chao Li[1,2,3,4], Michel Bouvier[6], Gunnar Schulte[5]✉ and Fei Xu[1,2,3,4]✉

[1]*iHuman Institute, ShanghaiTech University, Shanghai, China.* [2]*School of Life Science and Technology, ShanghaiTech University, Shanghai, China.* [3]*Center for Excellence in Molecular Cell Science, Shanghai Institutes for Biological Sciences, Chinese Academy of Sciences, Shanghai, China.* [4]*University of Chinese Academy of Sciences, Beijing, China.* [5]*Section of Receptor Biology & Signaling, Department of Physiology & Pharmacology, Karolinska Institutet, Stockholm, Sweden.* [6]*Institute for Research in Immunology and Cancer, Department of Biochemistry and Molecular Medicine, Université de Montréal, Montréal, QC, Canada.* [7]*Departments of Biological Sciences and Chemistry, Bridge Institute, University of Southern California, Los Angeles, CA, USA.* [8]*Present address: Orion Pharma R&D, Espoo, Finland.* [9]*These authors contributed equally: Lu Xu, Bo Chen, Hannes Schihada, Shane C. Wright*
✉*email: gunnar.schulte@ki.se; xufei@shanghaitech.edu.cn*

DATA AVAILABILITY

The cryo-EM 3D map of the FZD_7–mGs–Nb35 complex has been deposited in EMDB database with accession code EMD-31340; the coordinates have been deposited in PDB database with accession code 7EVW. The MD simulation data is available at www.gpcrmd.org with ID 245.

REFERENCES

1. Schulte, G. & Wright, SC. *Trends Pharmacol. Sci.* **39**, 828–42 (2018).
2. Taipale, J. & Beachy, PA. *Nature* **411**, 349–54 (2001).
3. Kozielewicz, P., Turku, A. & Schulte, G. *Mol. Pharmacol*. **97**, 62–71 (2020).
4. Phesse, T., Flanagan, D. & Vincan, E. *Cancers* **8**, https://doi.org/10.3390/cancers8050050 (2016).
5. Nehmé, R., Carpenter, B., Singhal, A., Strege, A., Edwards, PC. & White, CF. *PLoS ONE* **12**, e0175642 (2017).
6. von Maltzahn, J., Bentzinger, CF. & Rudnicki, MA. *Nat. Cell. Biol.* **14**, 186–91 (2012).
7. Wright, SC., Kozielewicz, P., Kowalski-Jahn, M., Petersen, J., Bowin, CF. & Slodkowicz, G. et al. *Nat. Commun*. **10**, 667 (2019).
8. Schihada, H., Shekhani, R. & Schulte, G. *bioRxiv* https://doi.org/10.1101/2021.02.05.429900 (2021).
9. Rasmussen, SG. et al. *Nature* **477**, 549–55 (2011).
10. Kozielewicz, P. et al. *Nat. Commun*. **11**, 414 (2020).
11. Yang, S. et al. *Nature* **560**, 666–70 (2018).
12. Valnohova, J., Kowalski-Jahn, M., Sunahara, RK. & Schulte, G. *J. Biol. Chem.* **293**, 17875–87 (2018).
13. Qi, X. et al. *Nature* **571**, 279–83 (2019).
14. Turku, A., Schihada, H., Kozielewicz, P., Bowin, CF. & Schulte, G. *Nat. Commun.* https://doi.org/10.1038/s41467-021-24004-z (2021).
15. Bowin, CF., Inoue, A. & Schulte, G. *J. Biol. Chem*. **294**, 11677–84 (2019).

ACKNOWLEDGEMENTS

This work was supported by the National Key R&D Program of China (2018YFA0507000 to F.X.), and the National Natural Science Foundation of China (32071194 to F.X.). Work at Karolinska Institutet was supported by Karolinska Institutet, the Swedish Research Council (2017-04676; 2019-01190), the Swedish Cancer Society (CAN2017/561, 20 1102 PjF, 20 0264P), the Novo Nordisk Foundation (NNF17OC0026940; NNF20OC0063168), The Swedish Society of Medical Research (SSMF; P19-0055), the Lars Hierta Memorial Foundation (FO2019-0086, FO2020-0304), The Alex and Eva Wallström Foundation for Scientific Research and Education (2020-00228), and the German Research Foundation (DFG, 427840891; KO 5463/1-1). S.C.W. is supported by a fellowship from the Swedish Society for Medical Research (P18-0098). Computational resources were provided by the Swedish National Infrastructure for Computing (SNIC 2020/5-500). M.B. is funded by the CIHR (FDN-148431) and holds a Canada Research Chair in Signal Transduction and Molecular Pharmacology. We thank Qiwen Tan, Lu Zhang, Junlin Liu, Na Chen, Qiaoyun Shi and Wei Xiao from iHuman Institute for protein cloning and expression support; Qianqian Sun, Yunhun Liu and Zhihui Zhang at the Bio-EM facility at ShanghaiTech University for technical support on data collection. We thank Vadim Cherezov from University of Southern California for advice on structure refinement.

AUTHOR CONTRIBUTIONS

L.X. performed cloning, protein purification, cryo-EM sample preparation, data collection and structure analysis; B.C. performed cryo-EM data processing, model building and refinement; Y.W. assisted with the structure analysis and some calculations; G.W.H. was responsible for structure quality control; X.Z. and C.L. characterized the protein expression at early phase of the project; H.S. and S.C.W. performed functional biosensor experiments; M.K.J. and P.K. performed FZD_7 construct mutagenesis for functional analysis; C.F.B. validated FZD_7 surface expression; A.T. performed the MD simulation and analysis and contributed to model interpretation and visualization. F.X. conceived the project. F.X. and G.S. designed, coordinated and supervised the experiments. L.X., B.C., S.C.W., H.S., M.B., G.S. and F.X. wrote the manuscript.

COMPETING INTERESTS

M.B. is the president of the scientific advisory board for Domain Therapeutics. M.B. has filed patent applications related to some of the biosensors used in this work and the technology has been licensed to Domain Therapeutics.

ADDITIONAL INFORMATION

Supplementary information The online version contains supplementary material available at https://doi.org/10.1038/s41422-021-00525-6.

Correspondence and requests for materials should be addressed to G.S. or F.X.

Reprints and permission information is available at http://www.nature.com/reprints